Comparative study of three modified sCO_2 Brayton recompression cycles based on energy and exergy analysis with GA optimisation

Chunlei Li and Qitai Eri*

School of Energy and Power Engineering,
Beihang University,
No. 37, Xueyuan Rd.,
Haidian District, Beijing, China
Email: lichunlei1996@126.com
Email: eriqitai@buaa.edu.cn
*Corresponding author

Abstract: As one popular supercritical CO_2 (sCO_2) power cycle, the recompression cycle has attracted various modifications. However, comparative studies are still required to determine whether these modifications are necessary. In this paper, three modifications on the original recompression cycle(I) are compared, which are reheating cycle(II), partial cooling cycle(III), and reheated partial cooling cycle(IV). Thermodynamic states are calculated based on the recuperator effectiveness, and the split ratio, reheating pressure and pre-cooling pressure are calculated by genetic algorithm (GA). The thermal efficiencies are calculated as 40.01%, 40.44%, 39.88%, and 41.63%. The exergy efficiencies are 55.49%, 56.07%, 55.27% and 57.69%. It reveals that only reheated partial cooling cycle improves the performance, neither reheating cycle nor partial cooling cycle. This conclusion is not limited to specific parameters as the parametric study indicates. One explanation from the exergy analysis is that the reheated partial cooling cycle combines the edges of both reheating and partial cooling modifications.

Keywords: sCO_2 Brayton cycle; recompression cycle; exergy analysis; genetic algorithm optimisation.

Reference to this paper should be made as follows: Li, C. and Eri, Q. (2021) 'Comparative study of three modified sCO_2 Brayton recompression cycles based on energy and exergy analysis with GA optimisation', *Int. J. Exergy*, Vol. 35, No. 2, pp.241–262.

Biographical notes: Chunlei Li is a Master's student at the School of Energy and Power Engineering, Beihang University, Beijing, China. He received his BSc at the School of Energy and Power Engineering, North China Electric University, Beijing, China. His interests cover supercritical CO_2 power cycles, thermodynamic modelling, exergy analysis, biomass gasification, computational fluid dynamics, and gas-solid multiphase flow.

Qitai Eri is a Professor with the School of Energy and Power Engineering, Beihang University, Beijing, China. His research areas are renewable energy, thermodynamics, biomass pyrolysis, and gasification, aerodynamics, heat transfer, and the inlets and nozzles of aero-engines. He has worked at Beihang University since 1995. He received his PhD at the Beihang University in 2009. He has published over 100 papers at academic conferences and international journals.

1 Introduction

Innovative design of power cycles has gained a lot of attention as a crucial way of further improving the efficiency of energy utilisation. In particular, the supercritical CO_2 (sCO_2) power cycle has become a strong candidate for replacing the conventional steam Rankine power cycle. The underlying concept involves replacing conventional working fluids (e.g., water, air) with sCO_2. Compared to the steam Rankine power cycle, sCO_2 cycle is more compact and more efficient. Compared to other non-steam working fluid for a power cycle, like He, CO_2 is cheaper and the study of the property of CO_2 is more adequate.

At present, the possible application of sCO_2 Brayton cycle is widely discussed, for example, in concentrated solar power plants (Xu et al., 2011; Zhang et al., 2007; Wang and He, 2017; Zhu et al., 2015; Turchi et al., 2018; Chacartegui et al., 2011; Bernagozzi et al., 2019). The sCO_2 Brayton cycle is also viewed as a promising candidate for nuclear power generation, and could potentially improve the safety and efficiency of next-generation nuclear power plants (Dostal et al., 2004; Serrano et al., 2017; Liu et al., 2019).

A number of studies about the sCO_2 cycle have been launched. In addition to the recompression cycle of Dostal, which was initially conceived and designed for the fourth generation nuclear power plants, a variety of configurations have been proposed (Liu et al., 2019). Sarkar (2009) conducted exergy and energy analyses on the recompression cycle. Reyes-Belmonte et al. (2016) showed that the recompression cycle is sensitive to recuperator effectiveness, with thermal efficiencies ranging from 40–50%. Atif and Al-Sulaiman (2017) conducted energy and exergy analyses at six different locations in Saudi Arabia from the sunlight to the electricity. Angelino introduced the partial cooling cycle, and further to this, Turchi compared simple recuperated cycle, recompression cycle and partial cooling cycle (Turchi et al., 2013; Neises and Turchi, 2014).

In comparative studies, fairness of comparison must be guaranteed; in the present study, the same baseline must be ensured for all four cycles. Variables can be classified as one of two types:

1 Fixed variables from which a higher (or lower) value infers an improvement in the final result (e.g., maximum cycle temperature, minimum cycle temperature, etc.)

2 Non-fixed variables with no definite influence on the final result (e.g., recompressed flow ratio, reheat pressure, partial pressure during cooling).

In this paper, the fixed variables are used as boundary conditions, while the non-fixed variables are considered operating parameters to be optimised. Therefore, two measures are adopted to guarantee fairness:

1 A set of unified, reasonable boundary conditions is determined according to the performance of each device from literature (Dostal et al., 2004; Bernagozzi et al., 2019; Reyes-Belmonte et al., 2016; Turchi et al., 2018; Neises and Turchi, 2014).

2 The genetic algorithm (GA) is used to optimise the operating parameters to ensure the best performance of each cycle can be achieved.

This paper first presents short descriptions of the four sCO_2 Brayton cycles. Then a mathematical model based on the first and second laws of thermodynamics is established. As an example, the base case is analysed, followed by validation using previously published results from the literature. Next, the parametric study is presented to verify the applicability of the base case conclusion. Finally, the main conclusions of the comparative study are summarised.

2 Power cycles descriptions

In this section, short descriptions of four sCO_2 Brayton cycles are provided. The four cycles are internally and logically linked. By taking the recompression (recomp) cycle as the main cycle, the influence of different variations on the recompression cycle are observed to assess whether the additional modifications improve the performance of the system: first, the reheating (reheat) cycle is examined to determine whether an additional reheating system is necessary; then, the partial cooling (parNoR) cycle is examined to determine whether the additional precooling and precompression steps are necessary; finally, the combined reheating and partial cooling (partialR) cycle is examined to determine whether the combination of reheating and partial cooling is advantageous.

2.1 Cycle (I): recompression cycle

The recompression cycle proposed by Dostal is adopted. The most unique design of the recompression cycle is that the flow is split into two streams before compression:

1 The stream passing through the main compressor (MC), accounting for $(1 - x)$ of the total mass of the flow, which passes through the cooler, MC, and low-temperature recuperator (LTR), before converging at the converging point.

2 The stream passing through recompressor, which only passes through the recompressor before converging.

The main advantage of this unique design is alleviation of the pinch-point problem of the LTR, thereby improving its effectiveness. Ordinarily, the minimum temperature difference will appear at the exit of a heat exchanger (HX). However, when a pinch point occurs, the minimum temperature difference will instead occur inside the HX. The reason for this phenomenon is that the heat capacities inside the LTR are unbalanced: the heat capacity of the cold side ($C_{p,c}$) is much higher than the heat capacity of the hot side ($C_{p,h}$), especially within the temperature range of the LTR. Moreover, the temperature difference between the two sides changes during the heat transfer process. The recompression cycle solves this problem by controlling the mass flow rate of the two sides to balance the discrepancy. Splitting the flow results in a lower mass flow rate on the cold side. The full flow passes through the hot side while only part of the flow ($1 - x$ of the full flow) passes through the cold side. Therefore, the heat capacity rate of the cold side, $(1-x)\dot{m}C_{p,c}$, and hot side, $x\dot{m}C_{p,h}$, can be balanced, alleviating the pinch-point problem.

Figure 1 (a) Layout of recompression cycle (b) T-s diagram

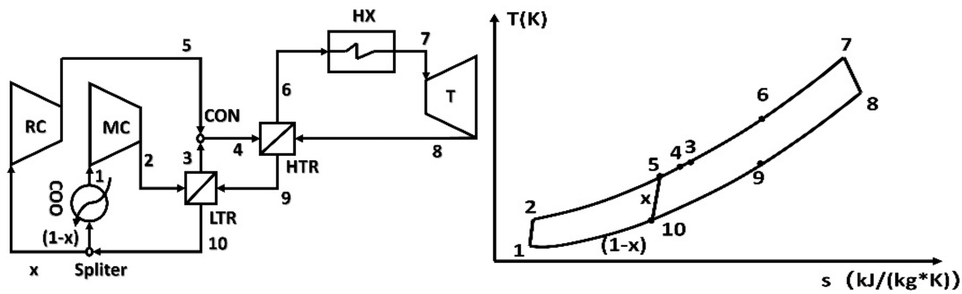

(a) (b)

2.2 Cycle (II): reheating cycle

Figure 2 shows the cycle layout (schematic diagram) and T-s diagram of the reheating cycle. By adding the reheating system, only the expansion process changes, i.e., state 7 to state 8. The expansion process is split into a high-pressure expansion process (7–1rh) and low-pressure expansion process (2rh–8). The reheating process is marked as 1rh–2rh. All other parts of the cycle remain the same.

Figure 2 (a) Layout of the reheating cycle (b) T-s diagram

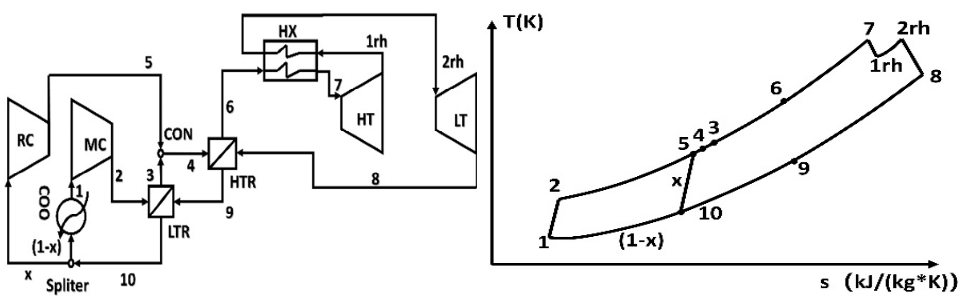

(a) (b)

2.3 Cycle (III): partial cooling cycle

The partial cooling cycle was proposed by Angelino, and can be defined as a recompression cycle with precompression and precooling processes. The purpose of precompression and precooling is to independently control state ‘a’. Since the pressure is independently controlled by the extra compressor, and the temperature is independently controlled by the extra cooler, state ‘a’ is free of the critical point (30.98°C, 7.377 MPa). This means the pressure and temperature of state ‘a’ may be much lower than the critical point, which will help the cycle generate more net work.

Figure 3 (a) Layout of partial cooling cycle (b) T-s diagram

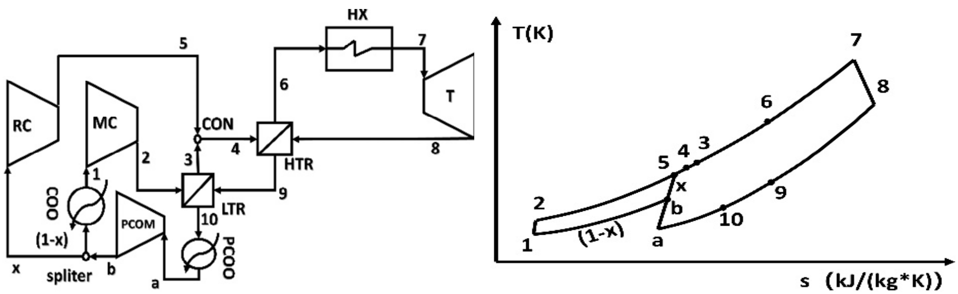

(a) (b)

2.4 Cycle (IV): reheated partial cooled cycle

Reheated partial cooling cycle is the combination of the former two cycles. Before the cooling process, it introduces precompressing and precooling procedures. After absorbing the heat process once, it introduces the reheating procedure.

Figure 4 (a) Layout of reheated partial cooling cycle (b) T-s diagram

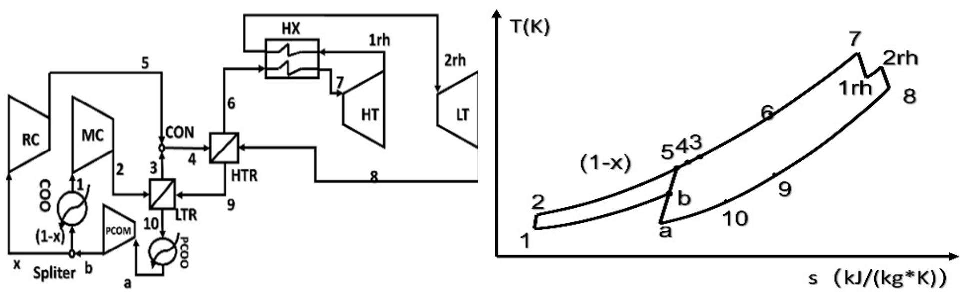

(a) (b)

3 Mathematical modelling

3.1 Model for recompression cycle

In this section, formulas for calculating the states at each point based on the first law of thermodynamics are presented. The aim of these calculations is to determine the temperature of each state. Then, the thermal efficiency and exergy efficiency can be calculated later.

Note that this section focuses on modelling the recompression cycle. The other three cycles will be modelled later, which requires only minor changes to the recompression cycle.

The isentropic efficiency of the turbines and compressors in the system can be defined, respectively, as follows:

$$\eta_T = \frac{actual\ expansion\ work}{isentropic\ expansion\ work}$$

$$\eta_c = \frac{isentropic\ compression\ work}{actual\ compression\ work}$$

Therefore, based on the turbine efficiency, states in expansion process are correlated. Similarly, the states in compression process are correlated. The following correlations can be derived:

$$h_8 = h_7 - \left(h_7 - h_{8s}\right)\eta_T \tag{1}$$

$$h_2 = h_1 + \left(h_{2s} - h_1\right)/\eta_c \tag{2}$$

$$h_5 = h_{10} + \left(h_{5s} - h_{10}\right)/\eta_c \tag{3}$$

Energy balance of recuperators:

$$heat\ absorbed\ in\ cold\ side = heat\ released\ in\ the\ hot\ side$$

For the high-temperature recuperator (HTR):

$$h_6 - h_4 = h_8 - h_9 \tag{4}$$

For the LTR:

$$(1-x)\left(h_3 - h_2\right) = h_9 - h_{10} \tag{5}$$

The definition of the effectiveness of recuperators:

$$\varepsilon = \frac{actual\ heat\ input}{theoretical\ maximum\ usable\ heat}$$

Here, formulas given by Reyes-Belmonte et al. (2016) are used. First, HTR and LTR effectiveness are defined, respectively, as

$$\varepsilon_{HTR} = \frac{Cp_h^H\left(T_8 - T_9\right)}{Cp_{\min}^H\left(T_8 - T_4\right)} = \frac{T_8 - T_9}{T_8 - T_4} \tag{6}$$

$$\varepsilon_{LTR} = \frac{Cp_h^L\left(T_9 - T_{10}\right)}{Cp_{\min}^L\left(T_9 - T_2\right)} \tag{7}$$

where

$$Cp_{\min}^H = \min\left(Cp_h^H, Cp_c^H\right) = Cp_h^H$$

$$Cp_{\min}^L = \min\left(Cp_h^L, (1-x)Cp_c^L\right)$$

are the smaller heat capacity of the hot side and cold side, respectively. In the HTR, the heat capacity of the hot side is always less than that of the cold side.

According to the energy balance, at the converging point, it has

$$(1-x)h_3 + xh_5 = h_4 \tag{8}$$

There are eight independent equations, equations (1)–(8). With the exception of the lowest state 1 and highest state 7, h1–h10 produce eight unknowns; thus, the equations have the only solution. However, the eight equations are nonlinear (especially for the HTR and LTR), therefore, an iterative method is required to solve them. A flowchart of the iterative method for solving the nonlinear equations as well as the solution strategy are presented in Appendix A.

When the working fluid passes through the cooler, HX, HTR, or LTR, the pressure will decrease due to friction and leak, etc. Thus, the pressure loss rate should be considered:

$$p_{out} = p_{in}\left(1-\Delta p_f\right) \tag{9}$$

The total heat absorbed and the total heat released during the cycles can be calculated, respectively, as

$$q_1 = h_7 - h_6, \tag{10}$$

$$q_2 = (1-x)\left(h_{10} - h_1\right) \tag{11}$$

Finally, the thermal efficiency can be calculated as

$$\eta_I = 1 - \frac{q_2}{q_1} \tag{12}$$

Assume the ambient temperature is T_0. The enthalpy under environment state is h_0. Entropy is s_0. The enthalpy of some arbitrary state is h, entropy is s. Thus, the enthalpic exergy of 1 kg of the working fluid in a specific state is

$$ex = h - h_0 - T_0\left(s - s_0\right) \tag{13}$$

The heat exergy absorbed is

$$ex_{Q1} = \left(1 - T_0/T_r\right)q_1 \tag{14}$$

The exergy loss of each equipment can be represented as

$$ir = ex_{in,component} - ex_{out,component} \tag{15}$$

Total exergy input of the power cycle is

$$\sum ex_{in,cycle} = ex_{Q1} \tag{16}$$

The exergy loss rate of each component in the cycle is

$$i = \frac{it}{\sum ex_{in,cycle}} \tag{17}$$

The exergy efficiency of the total power cycle is

$$\eta_{II} = 1 - \sum i \tag{18}$$

Another way of calculations of η_I and η_{II} is also presented here as follows.

$$\eta_I = \frac{w_t - w_{mc} - w_{rc}}{q_1} \tag{19}$$

$$\eta_{II} = \frac{w_t - w_{mc} - w_{rc}}{ex_{Q1}} \tag{20}$$

Equations (19) and (20) are equivalent to equations (12) and (18), respectively. Along with the equation (17), the correlation of η_I and η_{II} can be derived:

$$\eta_{II} = \eta_I \Big/ \left(1 - \frac{T_0}{T_r}\right) \tag{21}$$

Equations (12) and (18), instead of equations (19) and (18), are used to calculate the η_I and η_{II}. Equation (21) are used to examine the calculation by calculating η_{II} (renamed as η_{II}') from η_I. Such examination only checks the correctness of above formulas, and numerical errors may exist.

Given the total heat absorption Q_1, the net outputted work is:

$$W_{net} = Q_1 \eta_I \tag{22}$$

3.2 Formulas for the extra states in the reheating process and partial cooling process

To encompass reheating process and partial cooling process, two sets of formulas must be added: a set of equations to describe the additional states during reheating, i.e., 1rh and 2rh; another set of equation for describing the additional states during partial cooling, i.e., a and b.

For the reheating process, states 1rh and 2rh can be calculated using following formulas:

$$h_{1rh} = h_7 - \left(h_7 - h_{1rhs}\right)\eta_T \tag{23}$$

$$h_8 = h_{2rh} - \left(h_{2rh} - h_{8s}\right)\eta_T \tag{24}$$

For the partial cooling process, states a and b can be calculated, as follows:

$$h_a = h\left(P_{\min}, T_{\min}\right) \tag{25}$$

$$h_b = h_a + \left(h_{bs} - h_a\right)/\eta_c \tag{26}$$

Other formulas, such as q_1 and q_2, must also be modified, however, they are easily derived from the existing formulas and are not be listed here.

3.3 GA optimisation

As previously mentioned in the introduction, the GA played a crucial role in the present analysis. Every result went through the GA optimisation. The purpose was to obtain values of the operating parameters, other than the boundary conditions, and to optimise the performance of each cycle before performing the comparative analysis. Operating parameters of the four cycles are listed below:

- Variable of the cycle (I) recompression cycle: x.
- Variables of the cycle (II) reheating cycle: $x + P_{1rh}$.
- Variables of the cycle (III) particle cooling cycle: $x + P_a$.
- Variable of the cycle (IV) reheated partial cooling cycle: $x + P_{1rh} + P_a$.

The goal of optimisation:

$$\eta_{II}$$

where

- range of x is given as 0.2–0.4
- range of P_{1rh} is given as $P_{mc} - P_{\max}$
- range of P_a is given as 2.8 MPa – P_{mc} (keeping pressure ratio 2.67, 2.8 MPa = 7.5 MPa/2.67)
- range of T_a is given as $T_{\min} - T_{\max}$.

To determine whether a variable should be classified as an operating parameter (to be optimised) or an boundary condition (not optimised), the following rule can be adopted: if it is constrained by the performance of device and its effect on cycle efficiency is predictable, there is neither necessity nor justification to optimised it, thus it can be classified as a boundary condition; otherwise, it is considered as operating parameters.

For example, the compressor isentropic efficiency is considered as boundary condition, because the higher it is, the better performance of cycle can we predict. It totally depends on the device itself. If we take it as an optimised variable, then:

1. The fairness of comparison cannot be guaranteed, since the conditions of devices should not have difference.
2. The optimised compressor isentropic efficiency will very likely locate at its upper bound, which will make the optimisation meaningless.

Here, the GA function in MATLAB is adopted with a stopping criterion (relative change of fitness function) of 1e-6. This criterion is applied to wherever GA is used. To eliminate randomness of the GA, each result is calculated at least three times. If large discrepancies are observed after three tests (>0.1%), additional calculations are performed until at least three consistent values are obtained.

4 Results and discussion

The input parameters and corresponding results are presented in this section, as well as the data sources and an explanation of why each value was chosen as a parameter. All results were calculated in MATLAB, with the help of REFPROP 9.1. The results can be divided into two parts.

First, the base case is presented as a benchmark. A set of boundary conditions was chosen based on the current performance of the heat receiver, HX, and turbo-machinery. Data were obtained from literature. Then, the GA was used to obtain the operating parameters and to ensure maximum performance of each cycle under the boundary conditions, which also served as the basis of fair comparison. After the results were calculated, an exergy analysis was conducted on each component in each cycle. The results were then verified by comparing our results with previously published values that were obtained using the same set of boundary conditions.

Second, a parametric study was conducted. Nine parameters, $T_{\max}$, $P_{\max}$, $T_{\min}$, $P_{\min}$, P_{rest}, ε_{HTR}, ε_{LTR}, η_C and η_T were separately monitored and a total of 264 optimisation results were calculated using the GA. The input arguments and calculation method of the base case were used, and only the values of a single parameter were changed each time. The influence of each parameter on the exergy efficiency is presented as a line graph, followed by an analysis of the individual parameter and a general analysis.

4.1 Base case study

4.1.1 Boundary conditions for base case

The boundary conditions used in this study are presented in Table 1. The maximum temperature of the power cycle was set as the value of the most commonly used commercial heat transfer media, molten salt, which has a maximum temperature of 565°C (Dostal et al., 2004; Bernagozzi et al., 2019). In reality, the maximum temperature can vary due to the applications of different material of heat transfer fluid. This justifies the variation of $T_{\max}$ to examine its effect. The minimum temperature is 40°C in that critical point is 30.98°C. Compared to pressure, temperature is much harder to control, therefore, the temperature margin must be sufficient. If the temperature falls below the critical limit, the results could be disastrous for the compressor due to the possibility of phase changes inside the turbo machine. Therefore, the pressure was selected as 7.5 MPa, which gives a 5% margin of the critical pressure. Isentropic efficiencies of the turbines were selected according to the art-of-state value of turbo machinery for the sCO_2 Brayton cycle (Turchi et al., 2018). The isentropic efficiency of a compressor, i.e., η_C, was selected based on projection of mature and commercial size radial compressor (Neises and Turchi, 2014).

Table 1 Boundary conditions for the base case

Type	*Value*
$T_{\max}$ (°C)	550
$P_{\max}$ (MPa)	20
$T_{\min}$ (°C)	40
$P_{\min}$ (MPa)	7.5
Δp_f	2%
ε_{HTR}	0.95
ε_{LTR}	0.95
η_C	0.89
η_T	0.93

Table 2 Other parameters

Type	*Value*
T_0 (°C)	25
T_r (°C)	800
Q_1	600 MW

Except for the boundary conditions, other parameters (Table 2) should be given as well if the exergy analysis is adopted. The ambient temperature was selected as 25°C (De La Calle et al., 2018), and the heat source temperature was selected as 800°C (Sarkar, 2009), both are listed in Table 2. The total heat absorption is selected as 600 MW, which is used to calculated the output power. These parameters remained constant, and therefore did not affect the results of our analysis.

4.1.2 Validation of base case

The algorithm and code of the calculation procedure presented in Appendix A should be verified. Two verification methods were adopted:

1 Verify the η_{II} by the correlation of thermal efficiency and exergy efficiency, i.e., equation (24).

2 Compare the results with the results in the literature.

Note that all verifications were based on the recompression cycle and it was presumed that the other three cycle codes were also verified since they are based on modifications of the recompression cycle code.

Results of the first verification method, presented Table 3, show that the absolute values of η_{II} (calculated as one minus the sum of exergy loss rate of all devices) and η_{II}' (based on the correlation between first law efficiency and second law efficiency) only differ slightly (differences of less than 0.1%).

Table 3 Comparison with literature values

Type	*Value*
$T_{\max}$ (°C)	680
$P_{\max}$ (MPa)	24.8
$T_{\min}$ (°C)	40
P_{mc} (MPa)	7.8
Δp_f	1%
ε_{HTR}	0.95
ε_{LTR}	0.95
η_C	0.88
η_T	0.92
η_I (Reyes-Belmonte et al., 2016)	47.18%
η_I (Ma et al., 2019)	47.94%
η_I: this work	47.52%

The comparative analysis was also verified by the second method. Table 3 shows that our results are consistent with those previously published by Reyes-Belmonte et al. (2016) and Ma et al. (2019), with only minor discrepancies (<0.5%).

4.1.3 Results and exergy analysis of base case

Results of the base case are presented in Table 4 and Figure 5. Intuitively, it can be observed that:

1. The reheating process improves the performance of recompression cycle, however, the improvement is not large (only about 0.6%).
2. The partial cooling does not improve performance and on the contrary, may backfire.
3. The combination of reheating and partial cooling has an overall positive effect (2.2% improvement) on the performance of the recompression cycle.

Besides, data from the last column in Table 4 can shows that reheated partial cooling cycle improved 9.8 MW output work comparing to the recompression cycle. This improvement is greater than that of cycle II and cycle III.

Table 4 Base case GA optimisation results

Cycle	x	P_{1rh} *(kPa)*	P_a *(kPa)*	*Thermal efficiency* η_I	*Exergy efficiency* η_{II}	*Exergetic efficiency (verify)* η_{II}'	*Output work (MW)**
(I) Recomp	0.2401	-	-	40.01%	55.49%	55.41%	240.1
(II) Reheat	0.2342	13,348	-	40.44%	56.07%	56.00%	242.6
(III) ParNoR	0.3383	-	4,937	39.88%	55.27%	55.23%	239.3
(IV) PartialR	0.3265	9,554	4,268	41.63%	57.69%	57.64%	249.9

Note: *the total heat absorption is taken as 600 MW.

Figure 5 Base case efficiency of four cycles (see online version for colours)

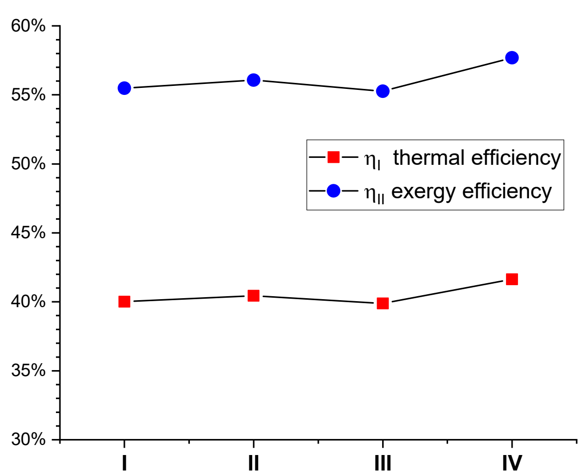

Note that in Table 4, η_{II}' represents the exergy efficiency calculated from the thermal efficiency, according to the equation (21) heat transfer relation, and can serve as a means of validating the results.

Figure 6 T-s diagrams of four cycles under the base case based on the calculated thermodynamic states, (a) recompression cycle (I) and reheating cycle (II) (b) recompression cycle (I) and partial cooling cycle (III) (c) recompression cycle (I) and reheated partial cooling cycle (IV) (see online version for colours)

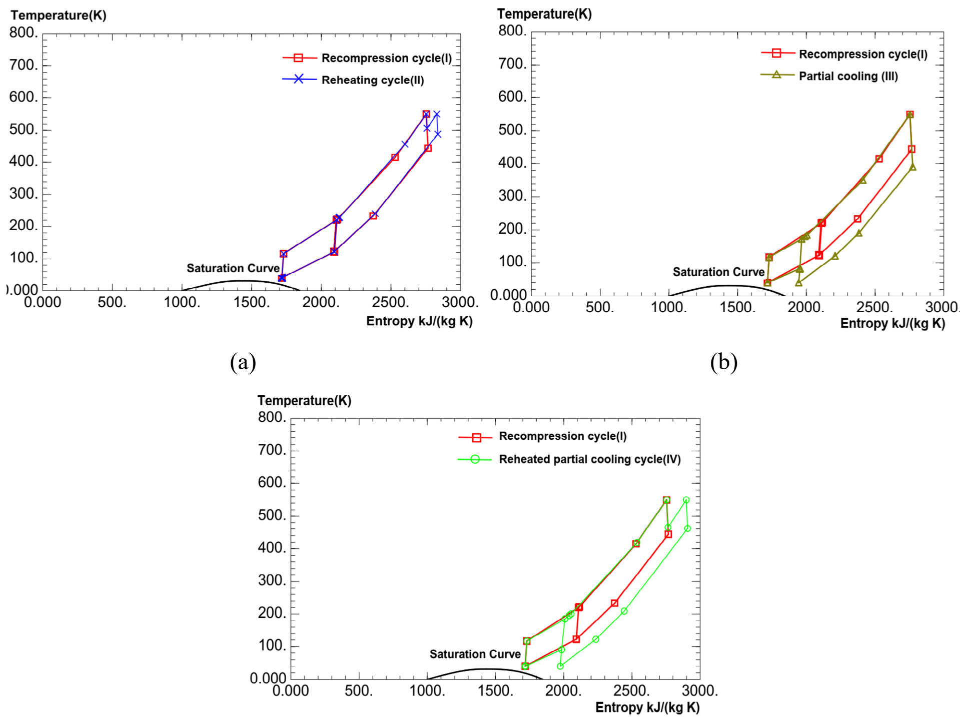

(a) (b)

(c)

Figure 6 compares the T-s diagrams of three modified cycles with the recompression cycle. Each cycle loop is overlaid with the recompression cycle to clearly show the difference. The parabola in the bottom centre represents the saturation line of CO_2, indicating that all states above this line are supercritical.

From the T-s diagram in Figure 6(a), it can be seen that cycle II (reheat) is almost the same shape as cycle I (recomp), apart from the additional reheating process in the right top corner. The additional area introduced by the reheating process corresponds to the extra work introduced into the cycle.

Compared to cycle III (parNoR), larger area is surrounded by cycle I (recomp) and it appears to be slightly 'fatter' because state 'a' is not constrained by the critical point (the pressure at 'a' is 4.937 MPa, which far lower than the critical pressure of 7.377 MPa). The lower pressure broadens the bottom edge of the cycle, which improves the efficiency; however, this is counteracted by the shift of the split point down along the bottom edge. This is also why the GA does not allow unrestricted downward movement of state ‘a’ until the point touches the lower boundary. Thus, the lower the pressure at ‘a’ does not improve the performance of the cycle.

Cycle IV (partialR) combines the cycle II (reheat) and cycle III (parNoR). On the one hand, the lower edge of the closed-loop is pulled down by descending state ‘a’. On the other hand, the area indicating the extra work introduced by the reheating process is enlarged owing to the downward shift of the lower edge. As a result, the increased work cancels out the negative effect of partial cooling, resulting in an increase in the overall efficiency of the cycle.

Figure 7 Exergy loss distribution of the base case, (a) group bar (b) stacked bar (see online version for colours)

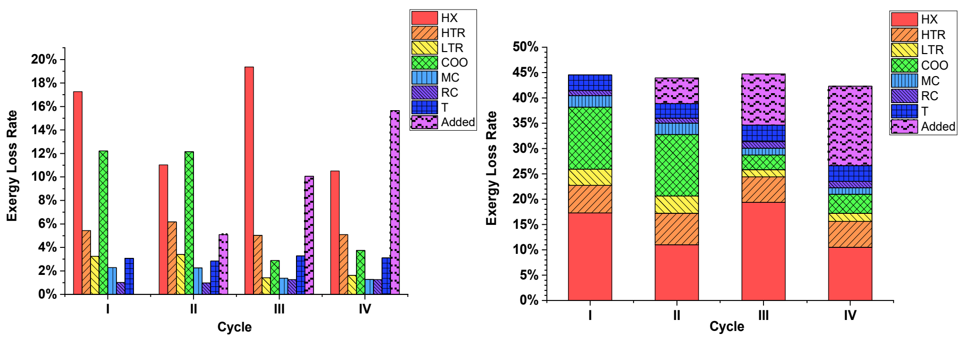

(a) (b)

Note: Normalised by ex_{Q1}.

‘Added’ refers to the added process compared to the original recompression cycle: In cycle II (reheating), the exergy loss during reheating; in cycle III (ParNoR), the exergy loss during recompression and precooling; in cycle IV (partial cooling), the exergy loss during the reheating and partial cooling process. The converger exergy loss is neglected since it is small.

As is shown in Figure 7, cycle I (recomp) and cycle II (reheat) have a similar exergy loss distribution. In both cases, the irreversibility of the HX and the cooler are responsible for the largest proportion of total exergy loss. Furthermore, the added exergy loss of reheater (marked as ‘added’ in Figure 7) in cycle II is coincidentally the reduced exergy loss in HX in cycle I, which may infer that the irreversibility is transferred from the HX to reheater but the total amount is unchanged.

Cycles III (parNoR) and IV (partial) exhibit the same patterns, as shown in Figure 7. Comparing the two cycles, their irreversibility distributions are similar. Irreversibility of the HX is still high, but unlike cycles I (recomp) and II (reheat), irreversibility of the cooler decreases considerably, and irreversibility of the HTR increases. Moreover, similar to cycles I (recomp) and II (reheat), part of the irreversibility of the HX is transferred to the reheater, however, the change in total irreversibility is small.

Comparing cycles I (recomp) and III (parNoR), the effect of the added partial cooling process can be observed. The total exergy loss greatly increases, and the main source of this increase is the HX and the added part (i.e., the partial cooling process). In addition, irreversibility of the cooler decreases a lot. This may be, in part, because the precooler and precompressor share the burden with the cooler during the low-temperature process.

However, adding the partial cooling process will greatly increase the total irreversibility. The key lies in whether this side effect is worth the gain in performance. The data presented in Table 3 and preliminary results of the parametric study suggest that the gain is worthwhile when the partial cooling is combined with reheating.

Figure 8 Variation of exergy efficiency with parameters, (a) effect of $T_{\max}$ (b) effect of $P_{\max}$ (c) effect of $T_{\min}$ (d) effect of $P_{\min}$ (e) effect of $1 - \Delta P_f$ (f) effect of ε_{HTR} (g) effect of ε_{LTR} (h) effect of η_C (i) effect of η_T (see online version for colours)

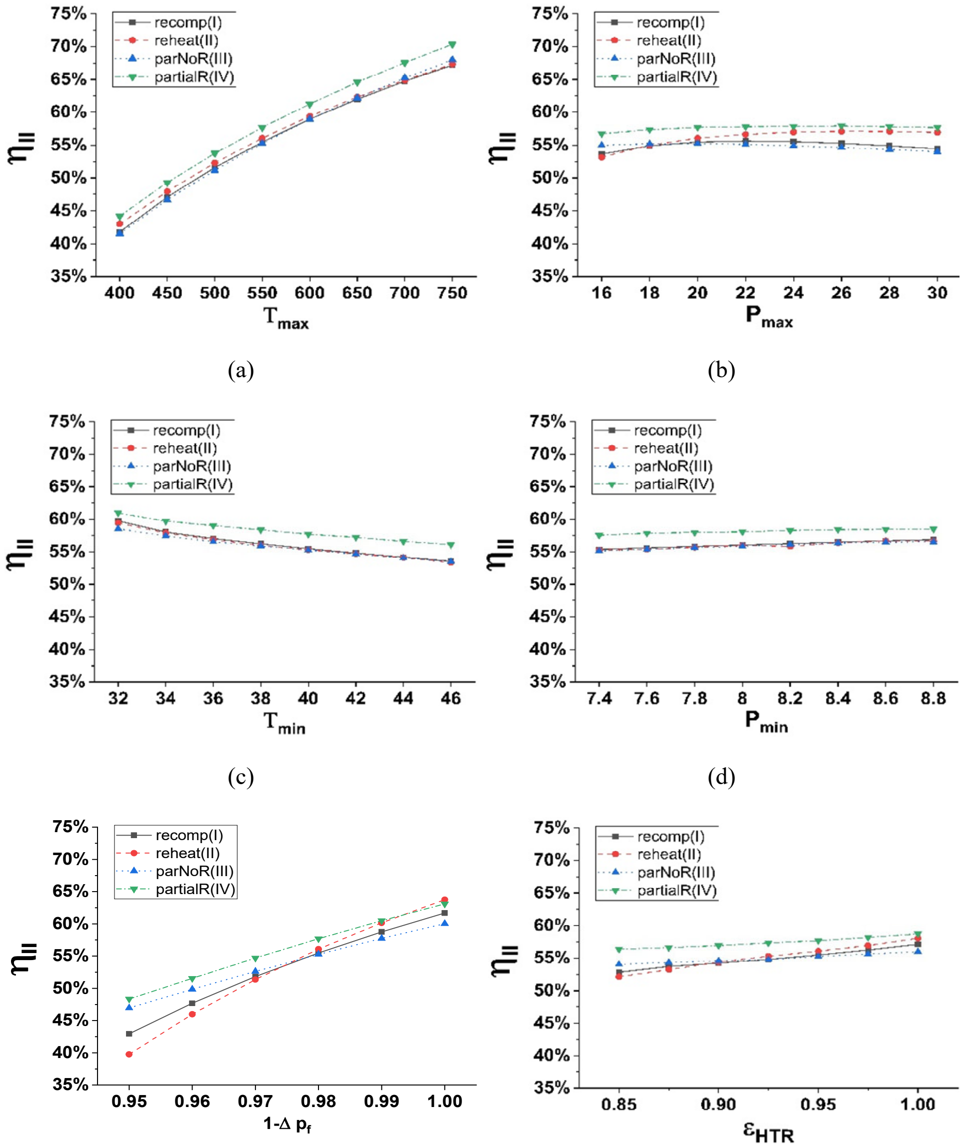

(a) (b)

(c) (d)

(e) (f)

Figure 8 Variation of exergy efficiency with parameters, (a) effect of $T_{\max}$ (b) effect of $P_{\max}$ (c) effect of $T_{\min}$ (d) effect of $P_{\min}$ (e) effect of $1 - \Delta P_f$ (f) effect of ε_{HTR} (g) effect of ε_{LTR} (h) effect of η_C (i) effect of η_T (continued) (see online version for colours)

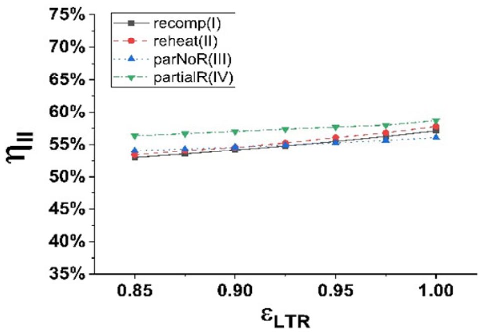

(g)

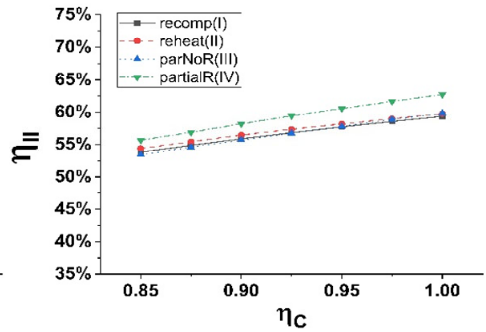

(h)

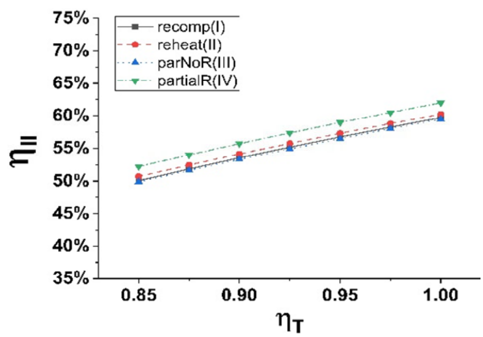

(i)

4.2 Parametric study

In this section, nine parameters (i.e., nine boundary conditions in base case) are analysed for each cycle. In total, 264 optimisation results were obtained. Each optimisation result is based on one parameter change while all other parameters remained the same.

Data are based on the average of three calculations to guarantee accuracy and eliminate minor randomness of the GA. If a discrepancy (>0.1%) was found among three calculations, extra calculation will be repeated to guarantee at least three calculated results are consistent for a single data point.

The effect of each parameter on the exergy efficiency is illustrated in Figure 8. In each graph, the y-axis remains unchanged, representing exergy efficiencies ranging from 35% to 75%, in order to intuitively compare the results.

As is shown in Figure 8, all parameters, except $P_{\max}$, have a positive influence on the exergy efficiency. The data were first compared vertically, i.e., to observe the influence of each parameter on a specific cycle. From the observation it can be seen that all four cycles exhibit similar trends under the influence of different parameters. Therefore, the recompression cycle was chosen as an example for discussion.

In Figures 8(a) and 8(b), in the recompression cycle, an obvious change in exergy efficiency can be observed if increasing the $T_{\max}$ from 400°C to 750°C, while in the meantime, increasing $P_{\max}$ from 16 MPa to 30 MPa will not greatly affect the exergy efficiency. The efficiency even goes down slightly when $P_{\max}$ is improved, reaching a maximum at 22 MPa or so. This phenomenon may be due to pressure loss through devices. When the maximum pressure increases and the pressure loss rate is unchanged, the absolute pressure drop in a device will increase; thus, the exergy loss in devices will increase and it makes the exergy efficiency decrease.

Figure 8(c) suggests that decreasing $T_{\min}$, towards the critical point, will improve the exergy efficiency as expectation. Whereas, Figure 8(d) shows that decreasing the pressure towards the critical point may not work for $P_{\min}$, as the curve remains roughly unchanged from 7.4 MPa to 8.8 MPa.

The last four graphs are more comparable than the first three since they change within the same range (0.85–1.00). In particular, the increase of ε_H and ε_L (performance indices of the HX recuperators), as shown in Figures 8(f) and 8(g) respectively, have the similar positive effect on the exergy efficiency. Similarly, the increase of η_C and η_T (performance indices of the turbo-machinery), as shown in Figures 8(h) and 8(i) respectively, also have the similar positive effect on the exergy efficiency. However, the amplifying effect of increasing η_T is apparently larger than that of η_C.

From a horizontal perspective, i.e., comparing the performance of the four cycles, one phenomenon is that the combination of reheating and partial cooling has an obvious effect on efficiency under the influence of all the parameters. This phenomenon proves that only adding reheating or partial cooling will have a minimal effect on the exergy efficiency of the sCO_2 recompression cycle, whereas combining them will have a much larger effect. This assertion may have exceptions for some values of $P_{\max}$ and P_{rest} ($P_{rest} = 1 - \Delta P_f$), where cycle II (reheat) achieved the equal or higher exergy efficiency.

5 Conclusions

In this paper, layouts of four cycles are compared, including recompression cycle, reheated recompression cycle, partial cooling cycle, and reheated partial cooling cycle. The sCO_2 recompression cycle was used as a reference, and other three cycles can be viewed as the modifications on the basis of recompression cycle. To ensure a fair and trustworthy comparison, a unified standard of comparison was proposed and two measures were adopted:

1 A set of uniform, reasonable, feasible boundary conditions were selected.

2 A set of operating parameters was so that every cycle is in their best performance under the same boundary condition.

The second step was performed with the aid of GA optimisation.

Based on the calculated results, bellowing conclusions can be drawn:

- The thermal efficiencies of four cycles (recompression cycle, reheating cycle, partial cooling cycle and reheated partial cooling cycle) are: 40.01%, 40.44%, 39.88% and 41.63%; the exergy efficiencies are: 55.49%, 56.07%, 55.27% and 57.69%.
- Reheating system only improves 0.43% thermal efficiency and 0.58% exergy efficiency because it just transferred the exergy loss from the HX to the reheater, while the neither the total exergy loss nor the exergy distribution changed

remarkably. The increase in reheating is due to the extra work introduced by the reheating process, however, the increase is not obvious since the extra area in the T-s diagram (corresponding to the extra work) is ‘slim’ and ‘narrow’.

- The partial cooling system cannot improve the performance because it introduces a great deal of exergy loss, which cancels out any improvement. Partial cooling makes the original closed-loop in the T-s diagram ‘fatter’ by shifting down the state ‘a’, but this advantage is cancelled out by the negative effect of simultaneously moving down the split point.
- Explanation of the success of the reheated partial cooling cycle (cycle IV) is: it combines the advantages of reheating and partial cooling. The ‘fatter’ loop broadens the area of extra work due to reheating, causing the extra yield to counteract any disadvantage.
- This conclusion was confirmed by the parameter study, which compared a total of 264 optimisation results for nine separately studied operating parameters: $T_{\max}$, $P_{\max}$, $T_{\min}$, $P_{\min}$, P_{rest}, ε_{HTR}, ε_{LTR}, η_C, η_T. In all nine of the line graphs presented in Figure 8, with the exception of some points of P_{rest} and $P_{\max}$, data indicate that reheated partial cooling cycle is superior to the other three power cycles In nearly all situations the reheated partial cooling cycle results in a 2–3% efficiency improvement on the original recompression cycle.

References

Atif, M. and Al-Sulaiman, F.A. (2017) ‘Energy and exergy analyses of solar tower power plant driven supercritical carbon dioxide recompression cycles for six different locations’, *Renewable and Sustainable Energy Reviews*, Vol. 68, pp.153–167, DOI: 10.1016/j.rser.2016.09.122.

Bernagozzi, M., Panesar, A.S. and Morgan, R. (2019) ‘Molten salt selection methodology for medium temperature liquid air energy storage application’, *Applied Energy*, Vol. 248, pp.500–511, DOI: 10.1016/j.rser.2016.09.122.

Chacartegui, R., Muñoz De Escalona, J.M., Sánchez, D., Monje, B. and Sánchez, T. (2011) ‘Alternative cycles based on carbon dioxide for central receiver solar power plants’, *Applied Thermal Engineering*, Vol. 31, No. 5, pp.872–879.

De La Calle, A., Bayon, A. and Soo Too, Y.C. (2018) ‘Impact of ambient temperature on supercritical CO_2 recompression Brayton cycle in arid locations: finding the optimal design conditions’, *Energy*, Vol. 153, pp.1016–1027, DOI: 10.1016/j.energy.2018.04.019.

Dostal, V., Driscoll, M.J. and Hejzlar, P. (2004) *A Supercritical Carbon Dioxide Cycle for Next Generation Nuclear Reactors*, Massachusetts Institute of Technology.

Liu, Y., Wang, Y. and Huang, D. (2019) ‘Supercritical CO_2 Brayton cycle: a state-of-the-art review’, *Energy*, Vol. 189, DOI: 10.1016/j.energy.2019.115900.

Ma, Y., Morozyuk, T., Liu, M., Yan, J. and Liu, J. (2019) ‘Optimal integration of recompression supercritical CO_2 Brayton cycle with main compression intercooling in solar power tower system based on exergoeconomic approach’, *Applied Energy*, Vol. 242, pp.1134–1154, DOI: 10.1016/j.apenergy.2019.03.155.

Neises, T. and Turchi, C. (2014) ‘A comparison of supercritical carbon dioxide power cycle configurations with an emphasis on CSP applications’, *Energy Procedia*, Vol. 49, pp.1187–1196.

Reyes-Belmonte, M.A., Sebastián, A., Romero, M. and González-Aguilar, J. (2016) 'Optimization of a recompression supercritical carbon dioxide cycle for an innovative central receiver solar power plant', *Energy*, Vol. 112, pp.17–27, Article number: 115900, DOI: 10.1016/j.energy.2019.115900.

Sarkar, J. (2009) 'Second law analysis of supercritical CO_2 recompression Brayton cycle', *Energy*, Vol. 34, No. 9, pp.1172–1178.

Serrano, I.P., Linares, J.I., Cantizano, A. and Moratilla, B.Y. (2017) 'A novel supercritical CO_2 power cycle for energy conversion in fusion power plants', *Fusion Science and Technology*, Vol. 64, No. 3, pp.483–487.

Turchi, C.S., Ma, Z., Neises, T.W. and Wagner, M.J. (2013) 'Thermodynamic study of advanced supercritical carbon dioxide power cycles for concentrating solar power systems', *Journal of Solar Energy Engineering*, Vol. 135, No. 4, Article number: 041007, DOI: 10.1115/1.4024030.

Turchi, C.S., Vidal, J. and Bauer, M. (2018) 'Molten salt power towers operating at 600–650°C: salt selection and cost benefits', *Solar Energy*, Vol. 164, pp.38–46, DOI: 10.1016/j.solener.2018.01.063.

Wang, K. and He, Y-L. (2017) 'Thermodynamic analysis and optimization of a molten salt solar power tower integrated with a recompression supercritical CO_2 Brayton cycle based on integrated modeling', *Energy Conversion and Management*, Vol. 135, pp.336–350, DOI: 10.1016/j.enconman.2016.12.085.

Xu, C., Wang, Z., Li, X. and Sun, F. (2011) 'Energy and exergy analysis of solar power tower plants', *Applied Thermal Engineering*, Vol. 31, Nos. 17–18, pp.3904–3913.

Zhang, X-R., Yamaguchi, H. and Uneno, D. (2007) 'Experimental study on the performance of solar Rankine system using supercritical CO_2', *Renewable Energy*, Vol. 32, No. 15, pp.2617–2628.

Zhu, Z., Zhang, D., Mischke, P. and Zhang, X. (2015) 'Electricity generation costs of concentrated solar power technologies in China based on operational plants', *Energy*, Vol. 89, pp.65–74, DOI: 10.1016/j.energy.2015.07.034.

Nomenclature

Abbreviations of cycles	
Recomp	Recompression cycle
Reheat	Reheat cycle
parNoR	Partial cooling cycle (without reheating)
partialR	Partial cooling cycle (with reheating)
Abbreviations of devices in layouts	
MC	Main compressor
RC	Recompressor
HTR	High temperature recuperator
LTR	Low temperature recuperator
T	Turbine
HT	High-pressure turbine
LT	Low pressure turbine
HX	Heat exchanger
COO	Cooler
PCOO	Precooler
PCOM	Precompressor
CON	Converger

Nomenclature (continued)

Thermodynamic states	
1	Inlet of MC
2	Outlet of MC. Inlet of LTR cold side
3	Outlet of LTR cold side
4	Inlet of HTR cold side. Outlet of converger
5	Outlet of recompressor
6	Inlet of HX
7	Outlet of HX
8	Outlet of turbine
9	Outlet of HTR hot side. Inlet of LTR hot side
10	Outlet of cooler
1rh	Inlet of reheating process
2rh	Outlet of reheating process
a	Inlet of precompressor
b	Outlet of precompressor
Thermodynamic quantities	
Pm	Pressure of state m
Tm	Temperature of state m
hm	Enthalpy of state m (1 kg)
sm	Entropy of state m (1 kg)
Others	
T_r	Heat source temperature
T_0	Ambient temperature
$T_{\max}$	Cycle maximum temperature. Or turbine inlet temperature
$P_{\max}$	Cycle maximum pressure. Or main-compressor outlet pressure
$T_{\min}$	Cycle minimum temperature. Or main-compressor inlet temperature
P_{mc}	Main-compressor inlet pressure
η_{II}	Exergy efficiency. Or the second law of thermodynamics efficiency
ε_{HTR}	Effectiveness of HTR
ε_{LTR}	Effectiveness of LTR
η_C	Isentropic efficiency of compressor
η_T	Isentropic efficiency of turbine
Δp_f	Pressure loss rate
x	Mass flow rate goes into RC (1 kg working fluid). Or ratio of stream in the sideway
ir	Specific exergy loss of a device
i	Exergy loss rate of a device
HB	Heat balance

Appendix A

Strategy for solving recuperators by effectiveness method

Figure A1 Schematic diagrams of flow in the LTR and HTR

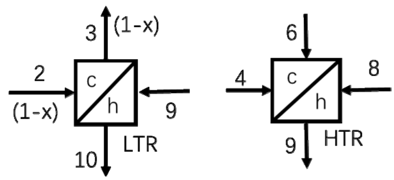

Notes: For HTR: T8 is given, solving the relationship between state 4, 6 and 9.

1 Assume T9, take the average of T8, T9 to get the $C_{p,h}$.
2 Solving T4 according to the HTR effectiveness equation, and look up h4 based on T4.
3 Solve h6 according to HTR heat balance, and look up T6.

For LTR: continue from last step, given T2.

6 Assume $C^L_{p,\min} = C^L_{p,h}$, solving T10 according to LTR effectiveness.
7 Solve h3 according to LTR heat balance, and look up T3.
8 Take the average of T3 and T2 as physical property, looking up the $C^L_{p,c}$.
9 Compare $C^L_{p,c}(1-x)$ with $C^L_{p,h}$, if $C^L_{p,h} < C^L_{p,c}(1-x)$, continue; otherwise, reassume $C^L_{p,\min} = C^L_{p,c}(1-x)$.

Figure A2 Flow chart of solving each state by iteration

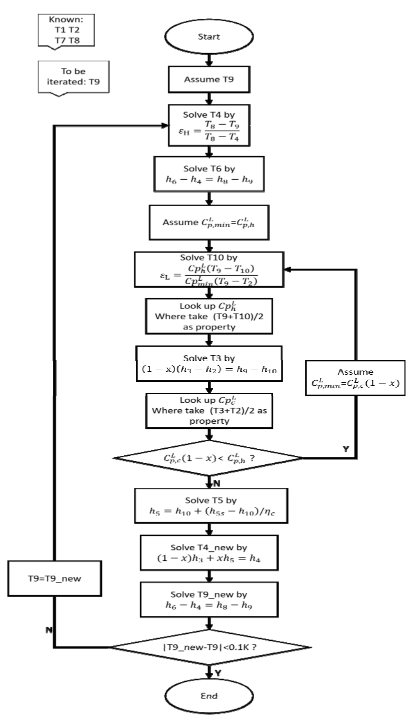

Appendix B

Results of base case in detail

Table B1 records the data of the base case, which gives the calculated thermodynamical states including temperatures and pressures at each state point. Table B2 records the data of exergy distribution of the base case.

Table B1 Thermodynamic states of base case

	I (recomp)		*II (reheat)*		*III (parNoR)*		*IV (partialR)*	
	T	*P*	*T*	*P*	*T*	*P*	*T*	*P*
1	40	7.5	40	7.5	40	7.5	40	7.5
2	116.4	20	116.4	20	116.4	20	116	20
3	222.6	19.6	228.5	19.6	182.1	19.6	200	19.6
4	222.1	19.6	226.7	19.6	177.5	19.6	195	19.6
5	220.2	19.6	220.7	19.6	168.4	19.6	185	19.6
6	415	19.2	456.4	19.2	356.2	19.2	419	19.2
7	550	18.8	550	18.8	550	18.8	550	18.8
8	444	8	488.1	8	397.3	5.2	462	4.5
9	233.2	7.8	239.8	7.8	188.4	5.1	209	4.4
10	122.2	7.7	122.6	7.7	120	5	122	4.4
1rh	-	-	506	13.3	-	-	465	9.6
2rh	-	-	550	7.5	-	-	550	9.4
a	-	-	-	-	40	4.9	40	4.3
b	-	-	-	-	77.3	7.7	90	7.7

Note: Units of temperatures are ℃, pressures are MP.

Table B2 Exergy loss distribution of four cycles in the base case

Cycle\IR	*HX*	*HTR*	*LTR*	*COO*	*MC*	*RC*	*T*	*Added*	*Sum*	*exQ1*
I (recomp)	20,721	6,522	3,901	14,654	2,738	1,218	3,687	-	53,406	119,985
II (reheat)	13,479	7,551	4,162	14,861	2,760	1,189	3,484	6,237	53,694	122,228
III (parNoR)	33,276	8,638	2,458	4,962	2,385	2,170	5,650	17,276	76,814	171,773
IV (partialR)	19,941	9,672	3,085	7,107	2,427	2,397	5,920	29,717	80,267	189,745

Notes: The units of IR are kJ/kg. ‘Added’ means reheater in II; precompressor and precooler in III; precompressor, precooler and reheater in IV.